Lathosterol Oxidase (Sterol C-5 Desaturase) Deletion Confers Resistance to Amphotericin B and Sensitivity to Acidic Stress in *Leishmania major*

Yu Ning,[a] Cheryl Frankfater,[b] Fong-Fu Hsu,[b] Rodrigo P. Soares,[c] Camila A. Cardoso,[c] Paula M. Nogueira,[c] Noelia Marina Lander,[d,e] ⓘ Roberto Docampo,[d,e] ⓘ Kai Zhang[a]

[a]Department of Biological Sciences, Texas Tech University, Lubbock, Texas, USA
[b]Mass Spectrometry Resource, Division of Endocrinology, Diabetes, Metabolism, and Lipid Research, Department of Internal Medicine, Washington University School of Medicine, St. Louis, Missouri, USA
[c]Fundação Oswaldo Cruz-Fiocruz, Instituto René Rachou, Belo Horizonte, Minas Gerais, Brazil
[d]Center for Tropical and Emerging Global Diseases, University of Georgia, Athens, Georgia, USA
[e]Department of Cellular Biology, University of Georgia, Athens, Georgia, USA

ABSTRACT Lathosterol oxidase (LSO) catalyzes the formation of the C-5–C-6 double bond in the synthesis of various types of sterols in mammals, fungi, plants, and protozoa. In *Leishmania* parasites, mutations in *LSO* or other sterol biosynthetic genes are associated with amphotericin B resistance. To investigate the biological roles of sterol C-5–C-6 desaturation, we generated an *LSO*-null mutant line (*lso⁻*) in *Leishmania major*, the causative agent for cutaneous leishmaniasis. *lso⁻* parasites lacked the ergostane-based sterols commonly found in wild-type *L. major* and instead accumulated equivalent sterol species without the C-5–C-6 double bond. These mutant parasites were replicative in culture and displayed heightened resistance to amphotericin B. However, they survived poorly after reaching the maximal density and were highly vulnerable to the membrane-disrupting detergent Triton X-100. In addition, *lso⁻* mutants showed defects in regulating intracellular pH and were hypersensitive to acidic conditions. They also had potential alterations in the carbohydrate composition of lipophosphoglycan, a membrane-bound virulence factor in *Leishmania*. All these defects in *lso⁻* were corrected upon the restoration of LSO expression. Together, these findings suggest that the C-5–C-6 double bond is vital for the structure of the sterol core, and while the loss of LSO can lead to amphotericin B resistance, it also makes *Leishmania* parasites vulnerable to biologically relevant stress.

IMPORTANCE Sterols are essential membrane components in eukaryotes, and sterol synthesis inhibitors can have potent effects against pathogenic fungi and trypanosomatids. Understanding the roles of sterols will facilitate the development of new drugs and counter drug resistance. LSO is required for the formation of the C-5–C-6 double bond in the sterol core structure in mammals, fungi, protozoans, plants, and algae. Functions of this C-5–C-6 double bond are not well understood. In this study, we generated and characterized a lathosterol oxidase-null mutant in *Leishmania major*. Our data suggest that LSO is vital for the structure and membrane-stabilizing functions of leishmanial sterols. In addition, our results imply that while mutations in lathosterol oxidase can confer resistance to amphotericin B, an important antifungal and antiprotozoal agent, the alteration in sterol structure leads to significant defects in stress response that could be exploited for drug development.

KEYWORDS *Leishmania*, amphotericin, drug resistance mechanisms, lipid synthesis, sterols, stress response

Leishmaniasis is the second most deadly parasitic disease, after malaria, with more than 12 million people infected worldwide (1). The causative agents belong to a group of trypanosomatid protozoans known as *Leishmania*. In the sandfly vector, *Leishmania* parasites are flagellated, extracellular promastigotes, whereas in the mammalian host, they are nonflagellated, intracellular amastigotes (2). Current treatments are limited by toxic side effects, and resistance is on the rise (3). Without a safe vaccine, it is necessary to identify new drug targets, develop new treatments, and decipher the mechanism of drug resistance in *Leishmania* (4).

The biosynthesis of sterol is an important pathway for most eukaryotes. In mammals, the dominant type of sterol is cholesterol, a vital membrane component that is also the precursor of steroid hormones (5). In fungi and trypanosomatids, ergostane-based sterols, such as ergosterol and 5-dehydroepisterol, are synthesized in high abundance and play roles equivalent to those of cholesterol in cellular membranes (6, 7). Ergosterol differs from cholesterol in the presence of two more double bonds: one at C-7–C-8 on the B ring and the other at C-22–C-23 on the side chain (see Fig. S1 in the supplemental material) (8). In addition, ergosterol has an extra methyl group at the C-24 position (Fig. S1). These structural differences make sterol biosynthesis a desirable source for antifungal and antitrypanosomatid drug targets.

Amphotericin B (Amp B) is a polyene antibiotic that binds to ergostane-based sterols on the plasma membrane of pathogenic fungi or *Leishmania*, leading to pore formation and the accumulation of reactive oxygen species (ROS) (9–11). It has been used successfully to treat antimony-resistant leishmaniasis and in patients coinfected with *Leishmania* spp. and human immunodeficiency virus (11, 12). However, resistance to Amp B has been reported both in the laboratory and in clinical isolates (13–16). Multiple Amp B-resistant *Leishmania* lines show altered sterol composition and mutations in sterol biosynthetic enzymes, such as the sterol C-24-methyltransferase (SMT; EC 2.1.1.41) and sterol C-14-alpha-demethylase (C14DM; EC 1.14.13.70) (13–16).

To interrogate the roles of these enzymes in *L. major*, we generated null mutants of C14DM ($c14dm^-$) and SMT (smt^-) using the targeted gene deletion approach (17). Both $c14dm^-$ and smt^- mutants lack ergostane-based sterols but are viable in culture and highly resistant to Amp B (18, 19). $C14dm^-$ mutants are extremely sensitive to heat and highly attenuated in virulence (19). They also display altered morphology, cytokinesis defects, and increased plasma membrane fluidity (19). In comparison, defects exhibited by smt^- mutants, including elevated mitochondrial membrane potential and superoxide level, are less drastic (18). Interestingly, both $c14dm^-$ and smt^- mutants show altered expression of lipophosphoglycan (LPG), a glycosylphosphatidylinositol (GPI)-anchored virulence factor (20). Compared to *L. major* wild-type (WT) parasites, the cellular level of LPG appears to be much lower in $c14dm^-$ but higher in smt^- mutants (18, 19). These findings suggest that loss-of-function mutations in C14DM and SMT can lead to Amp B resistance but result in significant defects in stress response and virulence.

In addition to C14DM and SMT, mutations in the gene encoding lathosterol oxidase (LSO) are also implicated in Amp B resistance in *Leishmania* and *Candida* spp. (15, 21, 22). LSO (also called sterol C-5-desaturase) catalyzes the formation of the C-5–C-6 double bond in the B ring of sterol intermediates, a late step in sterol synthesis (Fig. S1) (23). Orthologs of LSO have been identified in mammals, yeast, protozoans, plants, and algae (15, 23–26). In *Saccharomyces cerevisiae*, the activity of LSO (encoded by *ERG3*) is sensitive to cyanide and requires iron, NAD(P)H, and molecular oxygen (27). LSOs from yeast and *Tetrahymena thermophila* exhibit dependence on cytochrome b_5 and cytochrome b_5 reductase, suggesting that this desaturation reaction shares similarity to the sterol C-4- and C-14-demethylation steps (27–30) (Fig. S1).

In *S. cerevisiae*, deletion or inactivation of *ERG3/LSO* results in the accumulation of episterol and depletion of ergosterol, and the null mutants fail to grow in the absence of heme synthesis (23, 31) (Fig. S1). In addition, *ERG3/LSO* mutants are unable to utilize respiratory substrates, such as glycerol, acetate, and ethanol (25). Furthermore, LSO expression contributes to tolerance to high temperature and acidic pH in fission yeast
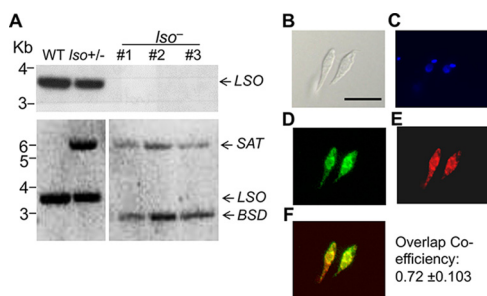
FIG 1 Genetic knockout and cellular localization of LSO. (A) Genomic DNA samples from *L. major* LV39 WT, *LSO*$^{+/-}$ (heterozygous knockout), and *lso*$^-$ (homozygous knockout clones 1 to 3) parasites were processed for Southern blot analyses, using radioactive probes from the open reading frame (top) or upstream flanking region (bottom) of *LSO*. Bands corresponding to *LSO* and drug resistance genes (*BSD/SAT*) are indicated. (B to F) Immunofluorescence microscopy of *lso*$^-$/+*LSO-GFP* promastigotes. (B) Differential interference contrast (scale bar, 10 μm). (C) DNA staining with Hoechst. (D) GFP fluorescence. (E) Anti-BiP (an ER marker) staining followed by goat anti-rabbit IgG-Texas Red. (F) Merge of panels D and E. Overlap between GFP and ER was calculated using JACoP Image J analysis from 30 cells.

(32). These studies allude to the functions of LSO in regulating respiration and stress response in fungi, although the mechanism of action is not well understood.

While LSO mutations were associated with Amp B resistance in fungi (21, 22), knockout mutants of LSO/Erg3 failed to display such resistance in *Candida albicans* and *Aspergillus fumigatus* (33, 34), questioning whether *LSO*-null mutation alone is sufficient to cause Amp B resistance. Studies on LSO in trypanosomatids are scarce. In light of its potential involvement in the development of Amp B resistance (15), it is necessary to characterize LSO in *Leishmania* and determine whether it is essential in the promastigote and amastigote stages and whether it is required for the sensitivity of *Leishmania* to sterol synthesis inhibitors or Amp B. To address these questions, we generated *LSO*-null mutants in *L. major*. Our results indicate that LSO deletion confers resistance to Amp B, but the mutants show poor survival and reduced growth rate under the acidic condition due to their inability to maintain intracellular pH. In addition, LSO deletion altered the structure of LPG and reduced parasite virulence in mice. These findings shed new light on the roles of sterol synthesis in *Leishmania* stress response and reveal the fitness costs associated with the development of drug resistance.

RESULTS

Genetic deletion and cellular localization of *L. major* LSO. The *L. major* LSO gene (TriTrypDB entry LmjF.23.1300) is located on chromosome 23 with 40% identity to *S. cerevisiae* ERG3p (gene ID 850745) and 38% identity to human sterol C-5-desaturase (GenBank accession no. BAA33729.1). The predicted open reading frame (ORF) contains 302 amino acids with four transmembrane helices and no obvious signal peptide, and it is expected to catalyze the formation of a double bond between C-5 and C-6 in the B ring of sterol intermediates (see Fig. S1 in the supplemental material).

To investigate the roles of the sterol C-5–C-6 desaturation reaction in *L. major*, we replaced the endogenous *LSO* alleles with nourseothricin (*SAT*) and blasticidin (*BSD*) resistance genes using the homologous recombination approach (17). The resulting *LSO*-null (*lso*$^-$) mutants were verified by Southern blotting with an ORF probe and a 5'-flanking sequence probe (Fig. 1A). To complement the null mutants, we introduced an LSO-expressing plasmid (pXG-LSO) into the *lso*$^-$ mutant to generate the *lso*$^-$/+*LSO* mutant (the add-back strain). To examine the cellular localization of LSO, the C terminus of LSO was fused to green fluorescent protein (GFP) and introduced into the *lso*$^-$ mutant (*lso*$^-$/+*LSO-GFP*) (Fig. S2A). In immunofluorescence microscopy, LSO-GFP showed a distribution similar (~72% overlap) to that of BiP, an endoplasmic reticulum (ER) marker (35) (Fig. 1B to F), suggesting that LSO is primarily located at the ER. This result is similar to the localizations of C14DM and SMT in *Leishmania* (18, 19) as well as LSO in *T. thermophila* (28).
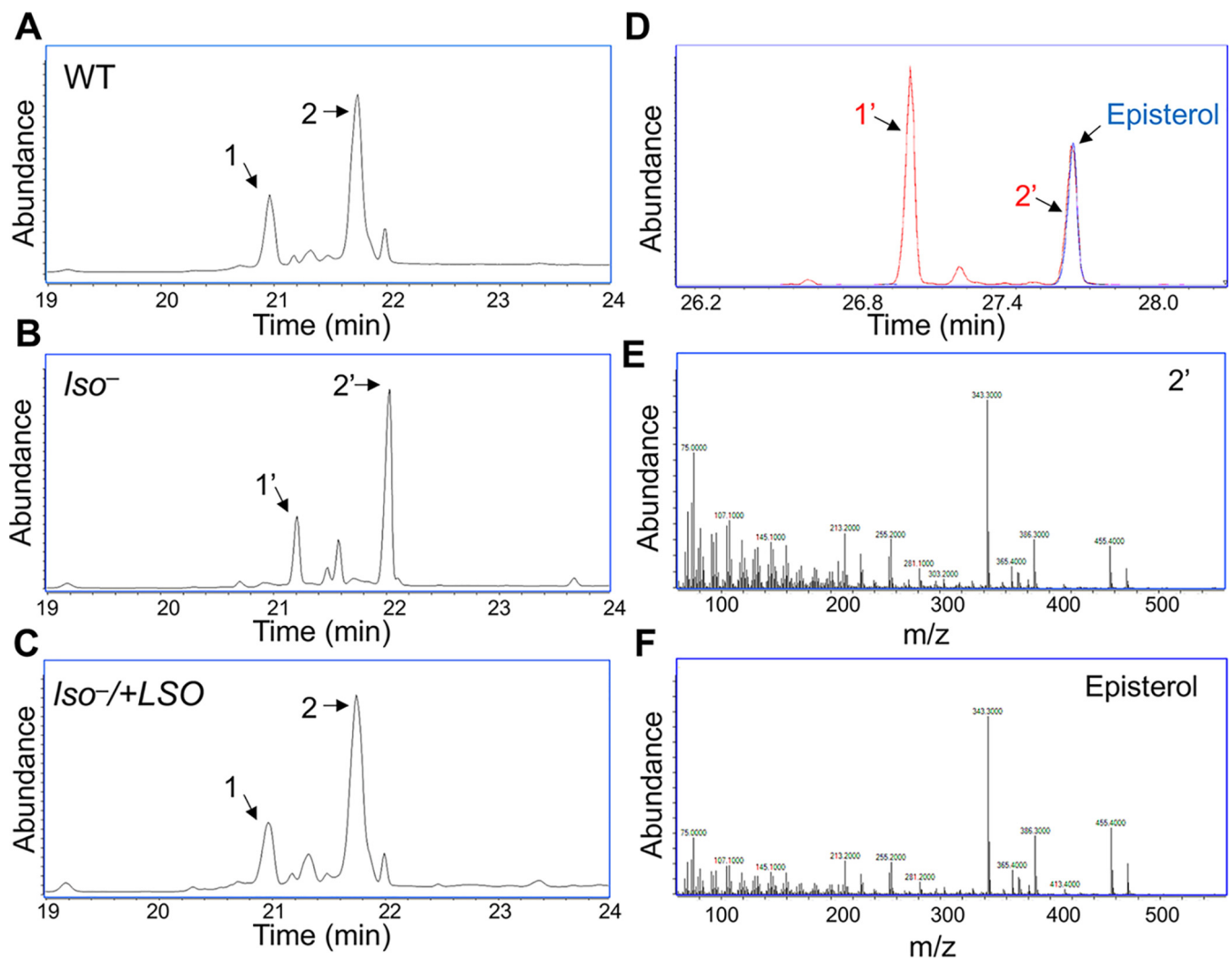
FIG 2 GC-MS analyses of sterol TMS derivatives show altered sterol profile in *Iso⁻* mutants. (A to C) Total ion current chromatograms plotted from 19.0- to 24.0-min scans (mass range, *m/z* 50 to 550) of the sterol TMS derivatives of LV39 WT (A), *Iso⁻* (B), and *Iso⁻/+LSO* (C) strains. In panels A and C, peaks 1 and 2 represent ergosterol and 5-dehydroepisterol, respectively. In panel B, the peaks including 1′ and 2′ are shifted to the right. (D) The reconstructed ion chromatogram of the M⁺ ion (*m/z* 470.5) from full GC-MS scans (*m/z* 50 to 550) of the *Iso⁻* sample (trace in red) and from the episterol standard (trace in blue). In addition to the perfect match of the retention time of peak 2′ with the episterol standard, the full-scan EI mass spectra (70 eV) plotted from peak 2′ (E) and the episterol standard (F) are also identical, confirming that peak 2′ is episterol.

Iso⁻ promastigotes have altered sterol composition. Sterols from promastigotes were converted into trimethylsilyl (TMS) derivatives, followed by electron ionization (EI) gas chromatography-mass spectrometry (GC-MS) analysis. Sterol molecules were identified based on their molecular weights, retention times, and EI spectra. Consistent with the findings we previously reported, *L. major* WT promastigotes contained two main sterols, i.e., ergosterol and 5-dehydroepisterol, represented by peaks 1 and 2, respectively, in Fig. 2A (18, 19). Interestingly, all the sterols from *Iso⁻* promastigotes were shifted to the right in the GC chromatogram, including two dominant peaks, 1′ and 2′ (Fig. 2B and Fig. S2B and C). While ergosterol and 5-dehydroepisterol had the expected molecular weight of 468.5 as TMS derivatives, the dominant sterols from the *Iso⁻* mutant (1′ and 2′) had the molecular weight of 470.5 as TMS derivatives (Fig. 2D). By library search, peak 1′ and peak 2′ matched ergosta-7,22-dien-3-ol, (3*β*,22E)- and episterol-TMS derivatives, respectively. While we did not have pure ergosta-7,22-dien-3-ol (3*β*,22E) (not available commercially) to confirm the structure of peak 1′, the retention time and the EI mass spectrum of peak 2′ in *Iso⁻* were identical to those of the episterol standard (Fig. 2D to F). These findings are consistent with the role of LSO
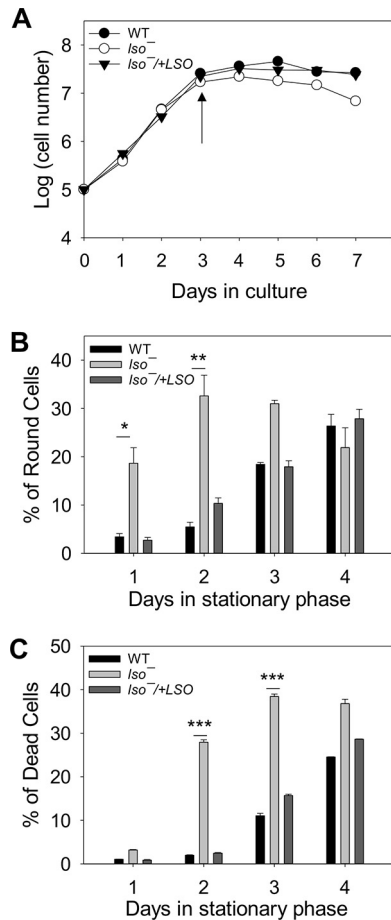
FIG 3 *Iso⁻* mutants show poor survival in stationary phase. (A) Promastigotes were inoculated in M199 medium at 1×10^5/ml, and cell densities were determined daily. The arrow marks the onset of stationary phase. (B and C) Percentage of round cells (B) and dead cells (C) were measured during days 1 to 4 in stationary phase. Error bars represent standard deviations from 3 experiments (**, $P < 0.01$; ***, $P < 0.001$).

in catalyzing the C-5–C-6 desaturation reaction to form 5-dehydroepisterol (Fig. S1). GC-MS analysis on the area ratios of internal standard peak and leishmanial sterol peaks revealed no significant difference in total cellular sterol abundance between WT and *Iso⁻* promastigotes. Importantly, the introduction of LSO or LSO-GFP into the *Iso⁻* strain restored the sterol profile to WT-like composition (Fig. 2C and Fig. S2). Taken together, these results support the identity of *L. major* LSO as a sterol C-5-desaturase.

Iso⁻ mutants are replicative in culture but show poor survival in stationary phase. The *LSO*-null mutants were fully viable in culture, with a doubling time of ~8 h during the log phase, and could reach a maximal density of 2×10^7 to 3×10^7 cells/ml, similar to WT and add-back parasites (Fig. 3A). However, after reaching maximal density, *Iso⁻* promastigotes showed significantly reduced viability in the stationary phase. First, we measured the percentage of cells whose long axis was less than twice the length of the short axis. Such a round shape was indicative of cells under duress. In early stationary phase (stationary days 1 to 2), 18 to 32% of *Iso⁻* promastigotes were round, whereas only 2 to 9% of WT and add-back cells were round (Fig. 3B). The difference became less pronounced in late stationary stage (stationary days 3 to 4) when the percentages of round cells increased among WT and add-back parasites (Fig. 3B). Similarly, we observed a much higher percentage of dead cells in *Iso⁻* mutants (28 to 38%) than in WT and add-back parasites (3 to 14%) from stationary day 2 to day 3 (Fig. 3C). We also examined the ability of *Iso⁻* mutants to form metacyclics, which are the nondividing and infective form of promastigotes (36). *Iso⁻* produced 40 to 50%
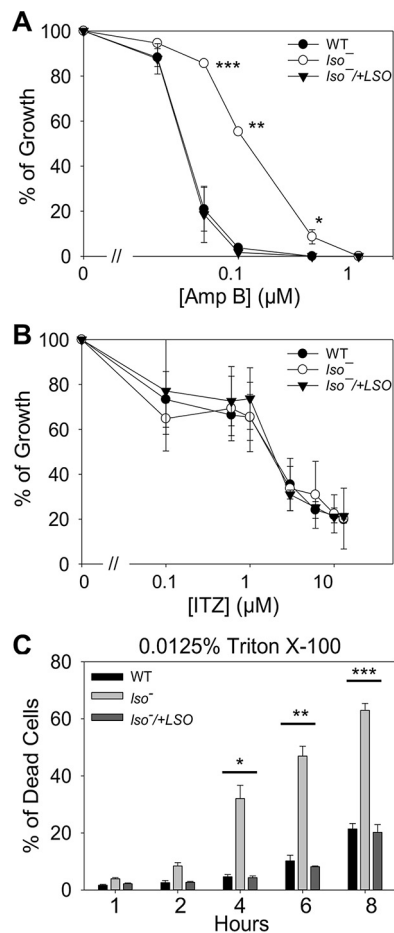
FIG 4 *Iso⁻* mutants are resistant to Amp B and hypersensitive to Triton X-100. (A and B) Log-phase promastigotes were inoculated into M199 medium with different concentrations of Amp B (A) or ITZ (B). Cells grown in the absence of drugs were used as controls, and percentages of growth were calculated after 48 h. (C) Log-phase promastigotes were incubated in the presence of 0.0125% Triton X-100 for 1 to 8 h. Cell viability was determined by flow cytometry. Error bars represent standard deviations from 3 to 4 experiments (*, $P < 0.05$; **, $P < 0.01$; ***, $P < 0.001$).

fewer metacyclics than WT and add-back parasites in stationary phase. In conclusion, LSO is not required for the survival or replication of log-phase promastigotes but is important for maintaining viability during the stationary phase.

Iso⁻ promastigotes show increased resistance to Amp B and are hypersensitive to Triton X-100. Amp B is a potent drug that interacts with ergosterol or ergosterol-like sterols on the plasma membrane, resulting in pore formation, oxidant accumulation, and cell death (9–11, 37). Alterations in sterol biosynthesis can confer resistance to Amp B (14, 16). In *Candida lusitaniae*, the Amp B-resistant clinical isolates showed reduced *ERG3* gene expression, suggesting that the C-5–C-6 double bond contributes to the binding of Amp B to membrane sterol (22). In another report, mutations in sterol C-5-desaturase (LSO) were found to be associated with Amp B resistance in *Leishmania mexicana* (15). Here, we measured the sensitivity of *Iso⁻* promastigotes to Amp B in liquid culture by growing cells in various concentrations of Amp B for 48 h (Fig. 4A). The effective concentrations to inhibit 25%, 50%, and 90% of growth (EC$_{25}$, EC$_{50}$, and EC$_{90}$, respectively) were determined using cells grown in the absence of Amp B as a control (Table 1). Compared to WT and *Iso⁻/+LSO* promastigotes, *Iso⁻* mutants were 2 to 4 times more resistant to Amp B (Fig. 4A and Table 1). The increase in Amp B resistance was close to that of the *smt⁻* mutants (18) but not as pronounced as that of the *c14dm⁻* mutants (10 to 100 times more resistant than the WT). This result is in agreement with the notion that C-5–C-6 desaturation enhances the binding between

TABLE 1 *lso⁻* mutants show reduced sensitivity to Amp B[a]

EC$_{25}$ (μM $\pm$ SD)			EC$_{50}$ (μM $\pm$ SD)			EC$_{90}$ (μM $\pm$ SD)		
WT	*lso⁻*	WT/*lso⁻*	WT	*lso⁻*	WT/*lso⁻*	WT	*lso⁻*	WT/*lso⁻*
0.034 $\pm$ 0.003	0.077 $\pm$ 0.004	1/2.24	0.046 $\pm$ 0.003	0.133 $\pm$ 0.005	1/2.89	0.084 $\pm$ 0.005	0.303 $\pm$ 0.033	1/3.61

[a]EC$_{25}$, EC$_{50}$, and EC$_{90}$ (averages $\pm$ standard deviations from 3 independent experiments) were calculated through comparison to control cells grown in the absence of Amp B.

membrane sterol and Amp B. Meanwhile, the susceptibility of *lso⁻* mutants to itraconazole, an inhibitor of C14DM (19), was similar to that of WT and *lso⁻/+LSO* parasites (Fig. 4B).

We also examined whether the change in sterol composition could alter the plasma membrane stability in *lso⁻* mutants. Log-phase promastigotes were incubated in regular medium containing 0.0125% Triton X-100, and percentages of dead cells were monitored over time. As shown in Fig. 4C, *lso⁻* exhibited hypersensitivity to Triton X-100 after 4 h, and the defect was rescued by the introduction of *LSO*. This finding resembles our previous observation in the *c14dm⁻* mutants, which are unable to form detergent-resistant membrane fractions (19). Therefore, alteration in sterol composition may cause hypersensitivity to detergent-induced plasma membrane disruption in *L. major*.

LSO is required for promastigote survival and optimal growth under acidic conditions. When promastigotes are transmitted from the sandfly vector to the mammalian host, they encounter elevated temperature, acidic pH, and oxidative bursts (38). Here, we investigated whether LSO is required for parasites to survive under stress conditions. First, promastigotes were inoculated in complete medium at pH 7.4 (the regular pH) or pH 5.0 for 0 to 60 h to examine their tolerance to acidic stress. While WT and *lso⁻/+LSO* cells showed good viability at pH 5.0 (<8% death), 25 to 30% of *lso⁻* mutants died after 8 to 12 h (Fig. 5A and B). The dead cell percentage in *lso⁻* mutants went down after 24 h (although still higher than those of WT and *lso⁻/+LSO* strains), which was likely due to the rapid lysis of dead cells (Fig. 5B). Next, we evaluated the ability of *lso⁻* promastigotes to withstand heat stress by increasing the culture temperature from 27°C to 37°C. As indicated in Fig. 5C, no significant difference was detected until 48 h into the temperature shift, when *lso⁻* mutants showed ~2 times more dead cells than WT and add-back parasites. We also incubated promastigotes in phosphate-buffered saline (PBS) to assess their resistance to starvation, and results indicated that the *lso⁻* mutants responded similarly to WT parasites (Fig. 5D).

Consistent with their hypersensitivity to acidic pH, *lso⁻* promastigotes proliferated slowly in the pH 5.0 medium (Fig. 5E). Overall, the mutants' poor survival and growth delay at pH 5 suggest that LSO is crucial for *L. major* promastigotes to tolerate acidic stress and affect parasite growth in the phagolysosome (39).

LSO contributes to intracellular pH homeostasis. Their hypersensitivity to acidic conditions prompted us to examine whether *lso⁻* mutants can regulate intracellular pH. When cultivated in the regular medium (pH 7.4), *lso⁻* mutants had a slightly lower intracellular pH than WT parasites (7.5 versus 7.8) (Table 2). However, when grown in an acidic medium (pH 5.0), the intracellular pH of the *lso⁻* mutant dropped to 7.0, whereas in WT and *lso⁻/+LSO* parasites it remained at 7.8 to 7.9 (Table 2). This finding argues that alteration in sterol composition can affect the cytosolic pH homeostasis in *L. major*.

The plasma membrane is the first barrier against the change of extracellular pH. Hypersensitivity of *lso⁻* mutants to Triton X-100 (Fig. 4C) suggests that their plasma membrane is less stable, thereby affecting their ability to control intracellular pH. Besides plasma membrane, certain intracellular organelles and proteins are essential for intracellular pH homeostasis as well (40). Acidocalcisomes are electron-dense acidic organelles rich in divalent cations and polyphosphate first identified in trypanosomatids (41). They play important roles in calcium homeostasis, osmoregulation, and the maintenance of intracellular pH (41, 42). The acidocalcisome has a vacuolar-type H$^+$-pyrophosphatase (VP1) that is involved in the uptake of H$^+$ from the cytosol into
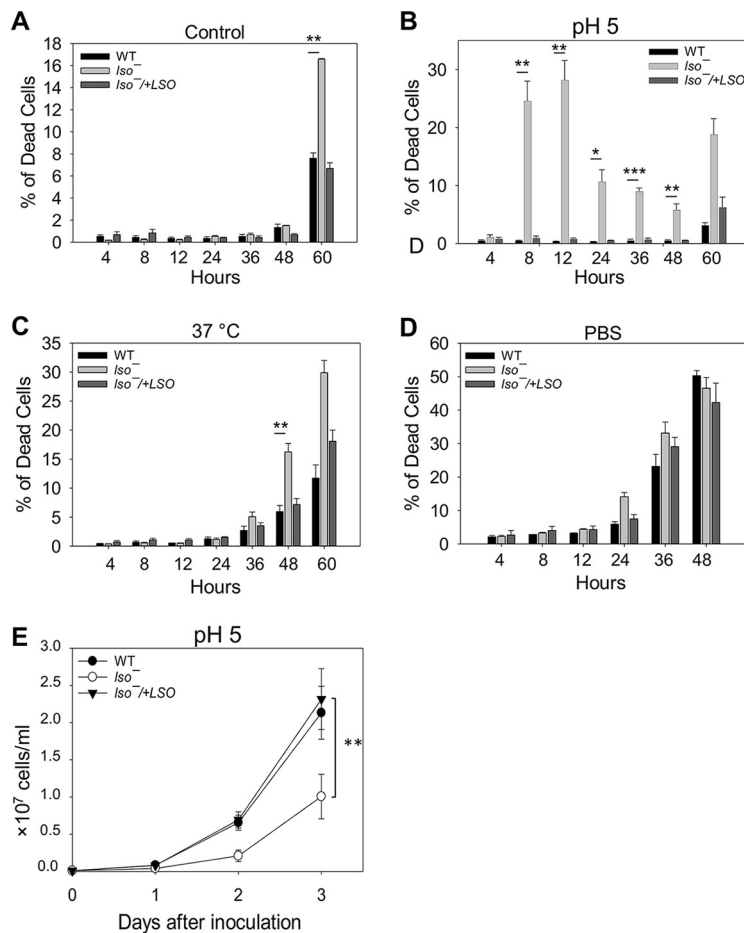
FIG 5 *Iso⁻* mutants show poor viability under acidic and heat stress. (A to D) Log-phase promastigotes were incubated at 5×10^6 cells/ml in M199 medium (A to C) or PBS (D) under neutral (A, C, and D) or acidic (B) conditions at either 27°C (A, B, and D) or 37°C (C). Percentages of dead cells were determined at the indicated times. (E) Log-phase promastigotes were inoculated into an acidic medium (pH 5.0) at 1×10^5 cells/ml, and culture densities were determined daily. Error bars represent standard deviations from 4 experiments (*, $P < 0.05$; **, $P < 0.01$; ***, $P < 0.001$).

acidocalcisomes and regulates intracellular pH homeostasis (43, 44). After labeling stationary-phase or metacyclic-like promastigotes with an anti-*T. brucei* VP1 antibody, we observed a 40 to 45% reduction in fluorescence intensity in *Iso⁻* mutants compared to that of WT and add-back parasites (Fig. 6A and B), suggesting that LSO is involved in the expression and/or localization of VP1 at the acidocalcisome. We did not detect any significant difference in acidocalcisome morphology, abundance, or contents in short-chain and long-chain polyphosphate between *Iso⁻* and WT parasites (Fig. S3A and B and data not shown). From these analyses, we postulate that compromised

TABLE 2 LSO is required for the maintenance of intracellular pH[a]

| | Intracellular pH at medium pH of: | | | |
| | 7.4 | | 5.0 | |
Cell type	Mean	SD	Mean	SD
WT	7.76	0.265	7.90***	0.122
Iso⁻	7.48	0.265	7.05***	0.031
Iso⁻/+LSO	7.83	0.124	7.78	0.130

[a]Promastigotes were cultivated in the regular medium (pH 7.4) or acidic medium (pH 5.0) for 3 days, and intracellular pH values were measured after labeling with 10 μM of BCECF-AM for 30 min. Mean values and standard deviations (SDs) were calculated from 3 experiments (***, $P < 0.001$).
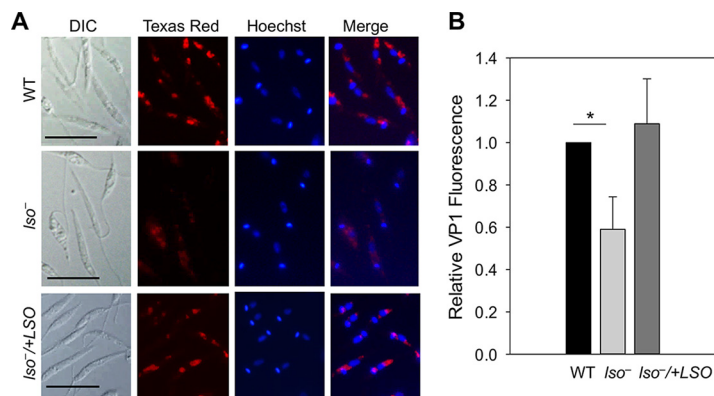
FIG 6 *Iso⁻* mutants express less vacuolar proton pyrophosphatase (VP1). (A) Day 3 stationary-phase promastigotes were labeled with rabbit anti-*Tb*VP1 antiserum (1:800), followed by anti-rabbit IgG-Texas Red (1:1,000). DNA was stained with Hoechst. DIC, differential interference contrast; merge, the merge of Texas Red and Hoechst images. Scale bar, 10 μm. (B) Relative levels of VP1 staining were determined from 100 metacyclic-like promastigotes for each line. Error bars represent standard deviations from 3 experiments (*, $P < 0.05$).

expression of VP1 along with increased plasma membrane instability in *Iso⁻* parasites contribute to their inability to maintain intracellular pH when challenged with acidic stress.

Depletion of *LSO* alters the expression and structure of LPG. Sterols are enriched in the ordered microdomains (lipid rafts) along with sphingolipids and glycosylphosphatidylinositol (GPI)-anchored proteins on the plasma membrane (45). Previous work on *c14dm⁻* and *smt⁻* mutants demonstrates that the alteration of sterol synthesis can affect the expression level of membrane-bound GPI-anchored virulence factors, such as LPG and GP63 (a metalloprotease) (18, 19). To determine the role of LSO in the synthesis of GPI-anchored glycoconjugates, we performed Western blot and immunofluorescence microscopy assays using the WIC79.3 monoclonal antibody, which recognizes the terminal Gal (β1,3) subunits on the side chains branching off the Gal (β1,4)-Man (α1)-PO₄ repeat units of *L. major* LPG (46, 47). As illustrated in Fig. 7A and B, whole-cell lysates from log-phase and stationary-phase *Iso⁻* parasites appeared to have less LPG than WT and *Iso⁻/+LSO* parasites (10 to 20% of the WT level) (Fig. 7E). The reduction was not due to increased release of LPG from *Iso⁻* parasites into the culture supernatant (Fig. 7A and B). Immunofluorescence microscopy assay confirmed this finding in *Iso⁻* mutants (Fig. 7G and H). Using the same WIC79.3 antibody, WT and add-back parasites displayed robust surface labeling at an exposure time of 100 ms (Fig. 7G). In contrast, signals from *Iso⁻* mutants were only detectable at a longer exposure time showing significant intracellular staining (Fig. 7H). Therefore, the expression of LPG was clearly altered in *Iso⁻* parasites. Meanwhile, these mutants showed levels of GP63 similar to those of WT and add-back parasites (Fig. 7C, D, and F).

LPG in *Leishmania* is a complex, polymorphic molecule composed of a lysoalkylphosphatidylinositol lipid anchor, a phosphorylated oligosaccharide core, a phosphoglycan backbone made of Gal (β1,4)-Man (α1)-PO₄ repeat units, which may contain side chains, and an oligosaccharide cap (20, 48). The lack of reactivity to WIC79.3 antibody in the *Iso⁻* mutant could reflect a loss or modification of side chains that branch off the phosphoglycan backbone (49, 50) or deficiencies in the synthesis of lipid anchor, oligosaccharide core, or phosphoglycan backbone (51, 52). To probe the LPG structure in *Iso⁻* parasites, we first carried out a Western blot analysis using the CA7AE monoclonal antibody, which recognizes the unsubstituted (bare) Gal (β1,4)-Man (α1)-PO₄ backbone (53). As shown in Fig. 8A, CA7AE could label the LPG and related proteophosphoglycan from *L. donovani* (strains lS2D and LV82), which was expected, since their phosphoglycan backbones were devoid of side chains (54). Meanwhile, no significant labeling was detected from *L. major* WT or *Iso⁻* parasites with the CA7AE antibody, suggesting that their LPG backbones had side chain modifications (Fig. 8A).
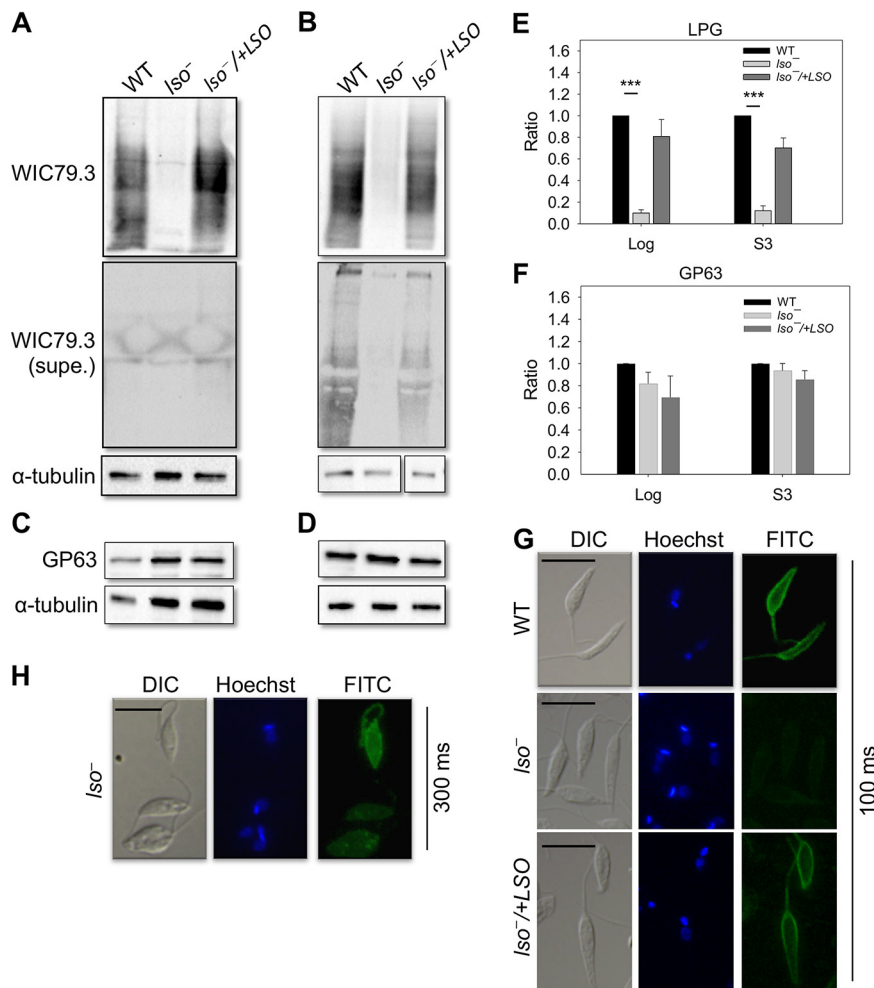
FIG 7 LSO is required for the synthesis of WT-like LPG. (A to D) Whole-cell lysates or culture supernatants (supe.) from log-phase (A and C) or day 3 stationary-phase (B and D) promastigotes were analyzed by Western blotting using anti-*L. major* LPG (MAb WIC79.3), anti-GP63, or anti-α-tubulin antibodies. (E and F) The relative abundance of LPG (E) and GP63 (F) in *Iso⁻* and *Iso⁻/+LSO* was normalized to the levels in LV39 WT promastigotes. Error bars represent standard deviations from 4 experiments (***, $P < 0.001$). (G and H) Log-phase promastigotes were labeled with MAb WIC79.3, followed by anti-mouse IgG-FITC. DNA was stained with Hoechst. Exposure times for the FITC channel were 100 ms (G) and 300 ms (H). Scale bar, 10 μm.

To explore the carbohydrate composition of the LPG side chain from *Iso⁻* mutants, we purified LPG from WT, *Iso⁻*, and *Iso⁻/+LSO* promastigotes as previously described (55). The yield of LPG was similar (150 to 200 μg/10¹⁰ cells for all lines), and these LPG samples exhibited reactivity similar to that of the WIC79.3 antibody, as we observed with whole-cell lysates (Fig. 7A and B and 8B). As expected, LPG from the *L. major* Friedlin V1 strain (positive control) was recognized strongly by this antibody (Fig. 8B) (50).

The LPG samples then were subjected to fluorophore-assisted carbohydrate electrophoresis (FACE) to analyze the sizes of their Gal (β1,4)-Man (α1)-PO$_4$ repeat units. As shown in Fig. 8C, *L. major* LV39 WT parasites had both short (G3 and G4) and intermediate (G5 to G11) side chains branching off the LPG repeat units, indicative of a mixture of mono-, di- ,and polygalactosylated residues on the side chains (49). Notably, *Iso⁻* mutants had a profile similar to that of the LV39 WT for the intermediate side chains (G5 to G11), but their short side chains (G3 and G4) were much reduced (Fig. 8C). As expected, *L. major* FV1 parasites had more short side chains (G3 and G4) than intermediate side chains (G5 to G11), which is consistent with the dominance of Gal1-2 short side chains capped with arabinose in this strain (Fig. 8C) (50, 56, 57).
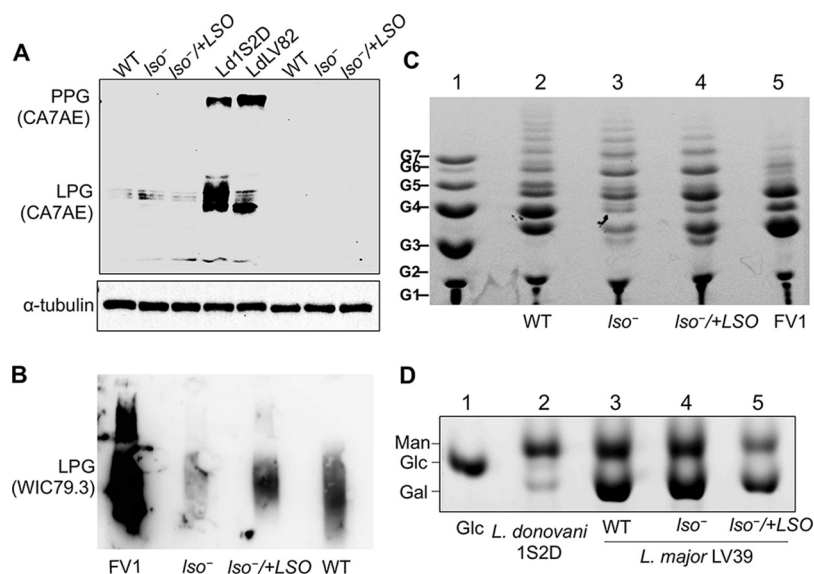
FIG 8 *Iso⁻* mutants have fewer short side chain sugar residues on their LPG. (A) Whole-cell lysates were processed for Western blotting with MAb CA7AE or anti-α-tubulin antibody. Log-phase (left three lanes) and day 3 stationary-phase (right three lanes) promastigotes of LV39 WT, *Iso⁻*, and *Iso⁻/+LSO* strains were analyzed along with *L. donovani* strains 1S2D and LV82 (middle two lanes). PPG, proteophospho-glycan. (B) Immunoblotting of purified LPG (5 μg per lane) from *L. major* strains probed with MAb WIC79.3. (C) FACE analysis of dephosphorylated LPG repeat units from *L. major* (lanes 2 to 5). Lane 1, malto-oligomer ladder represented by 1 to 7 glucose residues (G1 to G7). (D) Monosaccharide profile of GIPLs. Lane 1, glucose standard; lane 2, type I GIPL from *L. donovani* 1S2D containing mostly mannose residues and low levels of galactose; lane 3, repeat units of *L. major* LV39 WT (type II GIPL); lane 4, repeat units of *L. major* *Iso⁻*; and lane 5, repeat units of *L. major* *Iso⁻/+LSO*. Man, mannose; Glc, glucose; Gal, galactose. Experiments were performed twice, and results from one representative set are shown.

We next examined if LSO deletion affected the carbohydrate composition of gly-coinositolphospholipids (GIPLs), another major glycoconjugate in *Leishmania* (58). After strong acid hydrolysis, the carbohydrate composition of GIPLs was very similar among WT, *Iso⁻*, and *Iso⁻/+LSO* promastigotes, consistent with the galactose- and mannose-rich type II GIPLs (58, 59) (Fig. 8D). This profile was distinct from that of the type I GIPLs in *L. donovani*, which is highly enriched in mannose (59) (Fig. 8D). Together, these data suggest that LSO deletion does not change the carbohydrate profile of GIPLs but reduces the abundance of short (Gal1-2) side chains on the LPG backbone in *L. major*.

***Iso⁻* mutants have minor defects in the mitochondria.** Previous reports indicate that the inhibition of sterol biosynthesis can lead to compromised mitochondrial functions in trypanosomatids (18, 60–62). In *S. cerevisiae*, LSO/Erg3 is not required for viability in media containing ergosterol, but mutants fail to grow on nonfermentable substrates, such as glycerol and ethanol, suggesting that this enzyme is needed for respiration (31, 63). To assess the role of LSO in mitochondrial functions in *L. major*, we first examined the mitochondrial membrane potential ($\Delta\Psi_m$) after labeling cells with tetramethylrhodamine ethyl ester (TMRE) (64). Compared to WT and add-back para-sites, *Iso⁻* mutants had 30 to 50% higher $\Delta\Psi_m$ in the early stationary stage but did not show significant difference in log phase or late log phase (Fig. S4A). To measure the production of mitochondrial ROS, we labeled cells using a mitochondrion-specific ROS indicator, MitoSox Red. As shown in Fig. S4B, *Iso⁻* mutants had slightly higher fluores-cence signal than the WT and *Iso⁻/+LSO* parasites, although the difference was not statistically significant, except for that during log phase, suggesting a modest accumu-lation of ROS in their mitochondria. Next, we used the MitoXpress probe to examine oxygen consumption rate (65) by incubating log-phase promastigotes in a respiration buffer containing sodium pyruvate but no glucose. Under this condition, *Iso⁻* showed an oxygen consumption rate similar to that of WT and add-back parasites (Fig. S4C). Together, these data indicate that LSO deletion causes minor defects to the mitochon-dria in *L. major*.
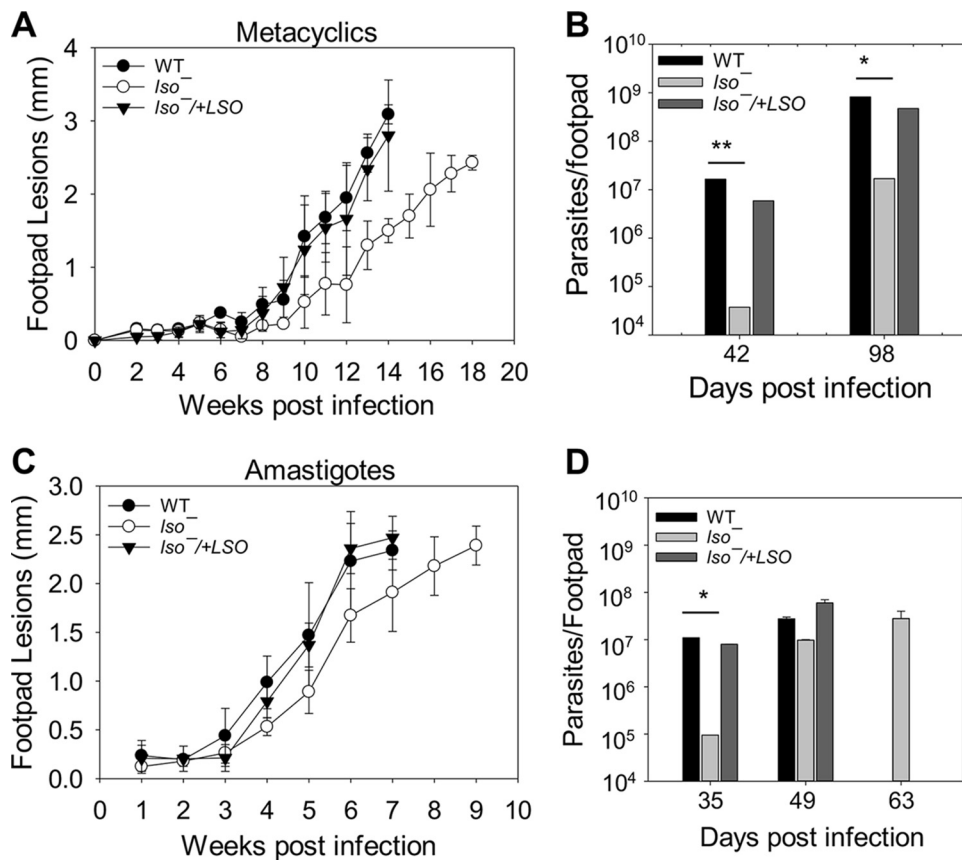
FIG 9 Iso⁻ mutants show attenuated virulence in mice. BALB/c mice were infected in the footpads with metacyclics (A and B) or amastigotes (C and D). Footpad lesions were measured weekly (A and C), and parasite numbers were determined by the limiting dilution assay (B and D). Error bars represent standard deviations (*, $P < 0.05$; **, $P < 0.01$).

Iso⁻ mutants show attenuated virulence in a mouse model.

To study the role of LSO in *L. major* virulence, metacyclics were isolated from stationary-phase cultures and used to infect BALB/c mice in the footpads. Parasite virulence was assessed by measuring the development of footpad lesions over time. Compared to WT and Iso⁻/+LSO parasites, mice infected by Iso⁻ mutants showed a 2- to 4-week delay in lesion progression (Fig. 9A), which was consistent with the lower parasite numbers in the infected footpads at weeks 6 and 14 postinfection (Fig. 9B). To explore the virulence of amastigotes, we isolated amastigotes from promastigote-infected footpads and used them to infect naive BALB/c mice. As shown in Fig. 9C and D, Iso⁻ amastigotes were slightly attenuated in virulence compared to those of WT and Iso⁻/+LSO amastigotes, but the difference was less pronounced than that of metacyclics. These findings suggest that LSO is important for *L. major* promastigotes to grow and cause disease in mice.

DISCUSSION

In this study, we characterized the gene encoding LSO (sterol C-5-desaturase), a sterol biosynthetic enzyme, in the protozoan parasite *L. major*. LSO catalyzes the formation of a double bond between C-5 and C-6 in the B ring of sterol intermediates (see Fig. S1 in the supplemental material). *L. major* LSO-null (Iso⁻) mutants were devoid of ergosterol or 5-dehydroepisterol (abundant in WT parasites). Instead, they accumulated C-5–C-6 saturated sterols such as ergosta-7,22-dienol and episterol (Fig. 2 and Fig. S2B to E). While the difference appears to be minor, Iso⁻ mutants were 2 to 4 times more resistant to Amp B than WT and Iso⁻/+LSO parasites (Fig. 4A and Table 1). These mutants were fully replicative in culture during the log phase but showed poor viability

after entering stationary phase (Fig. 3). LSO deletion also led to hypersensitivity to acidic pH (Fig. 5). These observations are largely in agreement with the phenotypes of the *ERG3* mutant in *S. cerevisiae* (23, 31).

It is interesting that LSO activity appears to contribute (directly or indirectly) to the binding affinity between Amp B and ergostane-based sterols. The C-5–C-6 double bond is conserved among all major sterols, including cholesterol (mammals), ergosterol (fungi and trypanosomatids), and stigmasterol (plants) (15, 23–26). Without this double bond, the A ring could twist/rotate more freely from the B ring, potentially making the sterol core less flat and reducing its binding capacity to Amp B (Fig. S1). Such a change in sterol core conformation could also increase the gap between sterol and phospholipid, making the membrane less stable. This is consistent with the increased sensitivity of *lso⁻* mutants to heat and Triton X-100 (Fig. 4C and 5C).

Compared to WT and add-back parasites, *lso⁻* mutants had a lower intracellular pH, and the difference became more pronounced when cells were cultivated in a pH 5.0 medium (Table 2). This finding is consistent with their reduced capacity to survive and replicate under the acidic conditions (Fig. 5B and E). Besides affecting the plasma membrane, the loss of LSO may influence the function of intracellular organelles, as sterols are located not only in the plasma membrane but also in the membrane of intracellular organelles. Acidocalcisomes are membrane-enclosed storage organelles involved in osmoregulation, phosphate metabolism, calcium homeostasis, and intracellular pH maintenance in protozoan parasites (41). The expression of VP1, an acidocalcisome-associated vacuolar H^+-pyrophosphatase, was lower in *lso⁻* parasites during stationary phase (Fig. 6). Since VP1 transports protons from the cytosol into acidocalcisomes (using pyrophosphate hydrolysis as the energy source), the reduced VP1 expression may lead to a more acidic intracellular pH and slower recovery of intracellular pH under acidic conditions (44).

Similar to the *C14DM*-null mutants, the cellular level of LPG in *lso⁻* parasites appeared to be significantly reduced based on Western blot and immunofluorescence microscopy analyses using the WIC79.3 antibody, which recognizes the terminal Gal (β1,3) subunits on the side chain of *L. major* LPG (46, 62) (Fig. 7 and 8B). However, further analyses suggest that *lso⁻* mutants still synthesized bulk glycoconjugates, as their LPG and GIPLs could be extracted and purified to yields similar to those of WT and add-back parasites (LPG, ~150 μg/10¹⁰ cells; GIPLS, ~60 μg/10¹⁰ cells). Lack of reactivity to CA7AE antibody indicates that the LPG backbone in *lso⁻* parasites is not bare like that in *L. donovani* (54) (Fig. 8A). In addition, the FACE result indicates that *lso⁻* mutants possess fewer short side chains and similar levels of intermediate side chains compared to those of WT parasites (Fig. 8C). Together, these data imply that the low WIC79.3 reactivity in *lso⁻* parasites is not due to a total loss of LPG structure, like several previously characterized LPG-biosynthetic mutants (51, 52, 66). Instead, it is likely caused by the reduced level of terminal Gal (β1,3) subunits on the LPG side chain. In *L. major*, certain groups of galactosyltransferases and arabinosyltransferases catalyze the attachment of galactose and arabinose, respectively, to the LPG side chains (49, 50). Future studies on the expression of these sugar transferases, along with detailed LPG structure determination in sterol mutants (*lso⁻*, *c14dm⁻*, and *smt⁻*), will help elucidate the molecular mechanism by which sterol synthesis influences LPG production in *Leishmania*.

Despite these defects, *lso⁻* parasites showed only slightly attenuated virulence in BALB/c mice (Fig. 9). While the hypersensitivity to acidic pH and heat likely compromised their ability to survive and replicate in the phagolysosome (39), these defects may be restricted to the promastigote stage and, thus, have only limited impact on disease progression after transitioning to amastigotes. Similarly, LPG is a known virulence factor for *L. major* promastigotes, but the structural change in *lso⁻* parasites may be relatively minor compared to those of LPG synthetic-null mutants (51, 67). Overall, the fitness loss displayed by *lso⁻* parasites is similar in severity to that of *smt⁻* and less dramatic than that of *c14dm⁻* mutants (18, 19).

Based on our characterization of the *smt⁻* and *lso⁻* mutants, it appears that

Leishmania could develop resistance to Amp B and only suffer mild to moderate fitness loss. However, Amp B has been used to treat leishmaniasis, especially visceral leishmaniasis (caused by *L. infantum* and *L. donovani*), since the 1960s, and reports of resistance have been scarce (4, 68). In addition, studies on several visceral leishmaniasis clinical isolates suggest that Amp B treatment failure is not due to resistance but other host/parasite factors (69, 70). Since our *smt⁻* and *lso⁻* mutants were generated in *L. major*, it would be of interest to determine the degree of fitness loss in equivalent mutants in *L. infantum* or *L. donovani*. While C14DM could be deleted from *L. major*, it is essential for *L. donovani* (19, 71), so perhaps *L. major* can better withstand changes in sterol synthesis than those responsible for visceral leishmaniasis infection.

In summary, our study shed new light on the biological roles of LSO in *Leishmania* sterol synthesis, growth, stress response, and virulence. Along with previous reports on *smt⁻* and *c14dm⁻* mutants (18, 19), these findings reveal the potential fitness costs associated with mutations conferring Amp B resistance and may offer strategies to counter the development of drug resistance.

MATERIALS AND METHODS

Materials. M199 medium, cholesta-3,5-diene, phenyl-Sepharose CL-4B, and alkaline phosphatase (from *Escherichia coli*) were purchased from Sigma-Aldrich (St. Louis, MO). Itraconazole (ITZ) and amphotericin B (Amp B) were purchased from LKT Laboratories, Inc. (St. Paul, MN), and EMD Chemicals, Inc. (San Diego, CA), respectively. MitoXpress oxygen probe was purchased from Luxcel Biosciences (Cork, Ireland). AG50W-X12 cation-exchange and AG1-X8 anion-exchange resins were purchased from Bio-Rad (Hercules, CA). All other chemicals were purchased from Thermo Fisher Scientific unless specified otherwise.

Molecular constructs. The predicted open reading frame (ORF) of *L. major LSO* (LmjF.23.1300, 302 amino acids) was amplified by PCR from *L. major* LV39 WT genomic DNA with primers 649 and 650 (see Table S1 in the supplemental material). The PCR product was digested with BamHI and ligated into the pXG vector to generate pXG-*LSO*. A modified ORF of *LSO* was amplified by using primers 649 and 651 to remove the stop codon and then used to generate pXG-*LSO*-GFP for localization study.

To generate knockout constructs, the upstream and downstream flanking sequences (~550 bp each) of *LSO* were amplified with primer pairs 645/646 and 647/659, respectively. These flanking sequences were digested and ligated into the cloning vector pUC18. Genes conferring resistance to nourseothricin (*SAT*) and blasticidin (*BSD*) were inserted between the upstream and downstream flanking sequences to generate pUC18-KO-*LSO*::*SAT* and pUC18-KO-*LSO*::*BSD*. All the molecular constructs were confirmed by restriction enzyme digestion and/or sequencing. Oligonucleotides used in this study are summarized in Table S1.

***Leishmania* culture and genetic manipulation.** Unless otherwise specified, *L. major* strain LV39 clone 5 (Rho/SU/59/P), *L. major* strain Friedlin V1 (MHOM/IL/80/Friedlin), *L. donovani* strain 1S2D (MHOM/SD/00/1S-2D), and *L. donovani* strain LV82 (MHOM/ET/67:LV82) promastigotes were cultivated at 27°C in M199 medium (pH 7.4, with 10% fetal bovine serum and other supplements) (72). The infective metacyclic promastigotes (metacyclics) were isolated from day 3 stationary-phase promastigotes using the density centrifugation method (73). To generate the *LSO*-null mutants, the two *LSO* alleles in *L. major* LV39 WT parasites were replaced with *BSD* and *SAT* by homologous recombination (17). The resulting heterozygous (*LSO⁺/⁻*) and homozygous (*lso⁻*) mutants were confirmed by Southern blotting. Briefly, genomic DNA samples were digested and resolved on a 0.7% agarose gel, transferred to a nitrocellulose membrane, and hybridized with [³²P]-labeled DNA probes targeting the ORF or a 500-bp upstream region of endogenous *LSO*. To restore *LSO* expression, pXG-*LSO* or pXG-*LSO*-GFP was introduced into *lso⁻* parasites by stable transfection, resulting in *lso⁻/+LSO* or *lso⁻/+LSO-GFP* parasites, respectively.

Sterol analysis by GC-MS. Total lipids were extracted from mid-log-phase promastigotes (3 × 10⁶ to 7 × 10⁶ cells/ml) by following the method of Folch et al. (74). An internal standard, cholesta-3,5-diene (formula weight, 368.34), was provided at 2.0 × 10⁷ molecules/cell during extraction. Lipid samples were dissolved in methanol at 1.0 × 10⁹ cell equivalents/ml. Equal amounts of each lipid extract in methanol were transferred to separate vial inserts, evaporated to dryness under nitrogen, and derivatized with 50 µl of BSTFA plus 1% TMCS-acetonitrile (1:3), followed by heating at 70°C for 30 min. GC-MS analysis was conducted on an Agilent 7890A GC coupled with Agilent 5975C MSD in electron ionization mode. Derivatized samples (2 µl each) were injected with a 10:1 split into the GC column with the injector and transfer line temperatures set at 250°C. The GC temperature started at 180°C and was held for 2 min, followed by 10°C/min increase until 300°C and then held for 15 min. To confirm that the unknown GC peak retention time matched that of the episterol standard, we also used a second temperature program started at 80°C for 2 min, ramped to 260°C at 50°C/min, held for 15 min, and increased to 300°C at 10°C/min and held for 10 min. A 25-m Agilent J & W capillary column (DB-1; inner diameter, 0.25 mm; film thickness, 0.1 µm) was used for the separation.

Immunofluorescence microscopy. For LSO-GFP localization, *lso⁻/+LSO*-GFP parasites were labeled with rabbit anti-*T. brucei* BiP antiserum (1:2,000) for 20 min, followed by goat anti-rabbit IgG-Texas Red antibody (1:1,000) for 20 min. Localizations of LPG were determined as previously described (19). To label acidocalcisomes, stationary day 3 promastigotes were permeabilized with ice-cold ethanol and stained

with rabbit anti-*T. brucei* VP1 (*Tb*VP1) antiserum (1:800) (44) for 30 min, followed by goat anti-rabbit IgG-Texas Red antibody (1:1,000). DNA staining was performed with 1.5 μg/ml Hoechst 33342 for 10 min. Images were acquired using an Olympus BX51 upright fluorescence microscope equipped with a digital camera. To quantify the overlap between LSO-GFP and anti-BiP staining, 30 randomly selected cells were analyzed using Image J JACoP (Just Another Colocalization Plugin) (75). The fluorescence intensity of *Tb*VP1 staining in WT, *lso*−, and *lso*−/+*LSO* parasites was measured from metacyclic-like cells (100 each) using Image J.

Cell growth, stress response, and drug sensitivity. To measure parasite growth under regular conditions, log-phase promastigotes were inoculated in M199 medium (pH 7.4) at 1.0×10^5 cells/ml and incubated at 27°C. Culture densities were determined daily using a hemocytometer. Percentages of round cells and metacyclics in stationary phase were determined as previously described (19). Parasite growth under the acidic condition was determined using an acidic M199 medium (same as complete M199 medium, except that the pH was adjusted to 5.0 with hydrochloric acid).

To assess cell viability under stress, mid-log-phase promastigotes were incubated in complete M199 medium (pH 7.4) at 37°C (heat stress) in an acidic M199 medium (pH 5.0) at 27°C (acidic stress) or in phosphate-buffered saline (PBS) at 27°C (starvation stress). Cell viability over time was determined by flow cytometry after staining with 5 μg/ml of propidium iodide (dead cells were highly positive for propidium iodide).

To determine sensitivity to drugs, log-phase promastigotes were inoculated in complete M199 medium at 2.0×10^5 cells/ml with different concentrations of Amp B (0.01 to 0.6 μM) or ITZ (0.01 to 13 μM). Percentages of growth were calculated after 48 h by comparing culture densities from drug-treated cells to cells grown in the absence of drugs (18).

To determine sensitivity to detergent, log-phase promastigotes were inoculated in complete M199 medium with 0.0125% Triton X-100 at 2.0×10^5 cells/ml. Cell viability was measured at different time points by flow cytometry after staining with propidium iodide.

Intracellular pH measurement. Intracellular pH was measured using a pH-sensitive fluorescent indicator, BCECF-AM (76). Briefly, promastigotes were inoculated in the regular (pH 7.4) medium or acidic (pH 5.0) medium at 1.0×10^5 cells/ml as described above. After 3 days, 1.0×10^7 cells were washed once with PBS and resuspended in 500 μl of buffer A (136 mM NaCl, 2.68 mM KCl, 0.8 mM MgSO$_4$, 11.1 mM glucose, 1.47 mM KH$_2$PO$_4$, 8.46 mM Na$_2$HPO$_4$, 1 mM CaCl$_2$, and 20 mM HEPES, pH 7.4) with 10 μM BCECF-AM. After 30 min of incubation, cells were washed twice and resuspended in buffer A. The emission intensity at 535 nm was measured using a microplate reader when samples were excited at 490 nm and 440 nm at the same time. The fluorescence intensity ratio (emission intensity at 535 nm when excited at 490 nm/emission intensity at 535 nm when excited at 440 nm) was converted into an intracellular pH value using a calibration curve, which was generated by measuring fluorescence intensity ratios of cells prepared in pH 5.0-pH 8.0 buffer A containing 10 μM BCECF-AM and 5 μg/ml the ionophore nigericin (77, 78).

Acidocalcisome isolation and analysis of short-chain and long-chain polyphosphate. Acidocalcisome fractions were isolated from log-phase and stationary-phase promastigotes as described for *T. brucei* and *T. cruzi* (79). The amounts of short-chain and long-chain polyphosphate in acidocalcisome fractions were determined as previously described (80).

Western blots. To determine LPG and GP63 expression, promastigotes were washed once in PBS and resuspended at 5.0×10^7 cells/ml in 1× SDS sample buffer. Samples were boiled for 5 min and resolved by SDS-PAGE, followed by immunoblotting with mouse-anti-*L. major* LPG monoclonal antibody WIC79.3 (1:1,000) (47), mouse-anti-GP63 monoclonal antibody 235 (1:1,000) (81), mouse-anti-*L. donovani* LPG monoclonal antibody CA7AE (1:500), or mouse-anti-α-tubulin antibody (1:1,000), followed by a goat anti-mouse IgG-horseradish peroxidase (1:2,000). To examine the expression of LSO-GFP, immunoblotting was performed using a rabbit anti-GFP antiserum (1:1,000) followed by a goat anti-rabbit IgG-horseradish peroxidase (1:2,000). To confirm LPG purification, 5 μg of purified LPG isolated from each strain was subjected to immunoblotting as described above using monoclonal antibody WIC79.3 (1:1,000).

Glycoconjugate extraction, purification, preparation, and FACE. LPG and GIPLs from *Leishmania* promastigotes (2 to 4×10^{10} cells each) were extracted in solvent E (H$_2$O-ethanol-diethyl ether-pyridine-NH$_4$OH; 15:15:5:1:0.017) and chloroform-methanol-water (10:10:3), respectively. The extracts were dried by N$_2$ evaporation, resuspended in 0.1 M acetic acid–0.1 M NaCl, and applied to a column of phenyl-Sepharose (2 ml), equilibrated in the same buffer. LPG and GIPLs were eluted using solvent E (82).

To prepare LPG repeat units, the LPG samples were depolymerized by mild acid hydrolysis (0.02 M HCl, 5 min, 100°C). This would generate a mixture of phosphorylated repeat units and core-PI anchor, which were separated after n-butanol–water (2:1) partitioning. Repeat units were collected in the aqueous phase and dephosphorylated with alkaline phosphatase in 15 mM Tris-HCl, pH 9.0 (1 U/ml, 16 h, 37°C). After enzymatic treatment, the repeat units were desalted by passage through a two-layered column of AG50W-X12 (H$^+$) over AG1-X8 (acetate) (55). GIPLs were depolymerized after strong acid hydrolysis (2 M trifluoroacetic acid, 3 h, 100°C) to obtain neutral monosaccharides, samples were dried in a speed-vac, and acid was removed by toluene wash (twice) under N$_2$. GIPL samples were resuspended in 500 ml of water and desalted as described above (59).

LPG repeat units and GIPL monosaccharides then were subjected to FACE analysis. Purified LPG samples were fluorescently labeled with 8-aminonaphthalene-1,3,6-trisulfate and subjected to FACE analysis, and the gel was visualized by a UV imager as described previously (55). To determine the monosaccharide composition of GIPLs, depolymerized and desalted GIPL samples were fluorescently labeled with 0.1 M 2-aminoacridone in 5% acetic acid and 1 M cyanoborohydride. Labeled sugars were

subjected to FACE, and the gel was visualized under UV light. Oligo-glucose ladders (G1 to G7) and monosaccharides (D-galactose, D-glucose, and D-mannose) were used as standards for oligosaccharides and monosaccharide gels, respectively (59).

Mitochondria membrane potential, mitochondrial ROS, and oxygen consumption. Mitochondrial membrane potential was determined as described previously (18). Log- or stationary-phase promastigotes were resuspended at 1.0×10^6/ml in PBS with 100 nM TMRE. After incubation at 27°C for 15 min, cells were washed once with PBS and analyzed by an Attune acoustic flow cytometer. To evaluate superoxide accumulation in mitochondria, promastigotes were resuspended in PBS at 1.0×10^7/ml and labeled with 5 μM MitoSox for 25 min. Cells were washed once with PBS and analyzed by flow cytometry (18). To determine the oxygen consumption rate, log-phase promastigotes were resuspended in a respiration buffer (Hanks' balanced salt solution with 5.5 mM sodium pyruvate, 5.5 mM 2-deoxy-D-glucose) at 2.0×10^7/ml, and oxygen consumption was measured with 1 μM MitoXpress as described previously (65). WT parasites treated with 10 μM antimycin A were included as a negative control (65).

Mouse footpad infection. BALB/c mice (female, 7 to 8 weeks old) were purchased from Charles River Laboratories International (Wilmington, MA). Mice were housed and cared for in a facility operated by the Animal Care and Resources Center at Texas Tech University. Procedures involving live mice were approved by the Animal Care and Use Committee at Texas Tech University (PHS-approved animal welfare assurance no. A3629-01). To determine parasite virulence, 2.0×10^5 metacyclics or 2.0×10^4 lesion-derived amastigotes were injected into the footpad of each mouse (5 mice per group). The progression of footpad lesions was monitored weekly using a Vernier caliper. Anesthesia was applied via isoflurane inhalation during footpad injection and measurement. Euthanasia was achieved by CO_2 asphyxiation. Parasite loads from infected footpads were determined by the limiting-dilution assay (83).

Statistical analysis. All experiments were repeated at least three times, except for the Southern blotting. All graphs were made using SigmaPlot 13.0 (Systat Software Inc, San Jose, CA). Differences between two groups were determined by the Student's t test. P values indicating statistical significance were grouped into values of <0.05 (*), <0.01 (**), and <0.001 (***).

SUPPLEMENTAL MATERIAL

Supplemental material is available online only.

FIG S1, PDF file, 0.4 MB.
FIG S2, PDF file, 0.7 MB.
FIG S3, PDF file, 0.3 MB.
FIG S4, PDF file, 0.04 MB.
TABLE S1, PDF file, 0.1 MB.

ACKNOWLEDGMENTS

REFERENCES

1. Desjeux P. 2004. Leishmaniasis: current situation and new perspectives. Comp Immunol Microbiol Infect Dis 27:305–318. https://doi.org/10.1016/j.cimid.2004.03.004.
2. Sunter J, Gull K. 2017. Shape, form, function, and Leishmania pathogenicity: from textbook descriptions to biological understanding. Open Biol 7:170165. https://doi.org/10.1098/rsob.170165.
3. Croft SL, Olliaro P. 2011. Leishmaniasis chemotherapy–challenges and opportunities. Clin Microbiol Infect 17:1478–1483. https://doi.org/10.1111/j.1469-0691.2011.03630.x.
4. Ponte-Sucre A, Gamarro F, Dujardin J-C, Barrett MP, López-Vélez R, García-Hernández R, Pountain AW, Mwenechanya R, Papadopoulou B. 2017. Drug resistance and treatment failure in leishmaniasis: a 21st century challenge. PLoS Negl Trop Dis 11:e0006052. https://doi.org/10.1371/journal.pntd.0006052.
5. Payne AH, Hales DB. 2004. Overview of steroidogenic enzymes in the pathway from cholesterol to active steroid hormones. Endocr Rev 25:947–970. https://doi.org/10.1210/er.2003-0030.
6. Goad LJ, Holz GG, Jr, Beach DH. 1984. Sterols of Leishmania species. Implications for biosynthesis. Mol Biochem Parasitol 10:161–170. https://doi.org/10.1016/0166-6851(84)90004-5.
7. Parks LW. 1978. Metabolism of sterols in yeast. CRC Crit Rev Microbiol 6:301–341. https://doi.org/10.3109/10408417809090625.
8. Cournia Z, Ullmann GM, Smith JC. 2007. Differential effects of cholesterol, ergosterol and lanosterol on a dipalmitoyl phosphatidylcholine membrane: a molecular dynamics simulation study. J Phys Chem B 111:1786–1801. https://doi.org/10.1021/jp065172i.
9. Lemke A, Kiderlen AF, Kayser O. 2005. Amphotericin B. Appl Microbiol Biotechnol 68:151–162. https://doi.org/10.1007/s00253-005-1955-9.
10. Mesa-Arango AC, Trevijano-Contador N, Román E, Sánchez-Fresneda R, Casas C, Herrero E, Argüelles JC, Pla J, Cuenca-Estrella M, Zaragoza O. 2014. The production of reactive oxygen species is a universal action mechanism of amphotericin B against pathogenic yeasts and contributes to the fungicidal effect of this drug. Antimicrob Agents Chemother 58:6627–6638. https://doi.org/10.1128/AAC.03570-14.

11. Jha TK, Giri YN, Singh TK, Jha S. 1995. Use of amphotericin B in drug-resistant cases of visceral leishmaniasis in north Bihar, India. Am J Trop Med Hyg 52:536–538. https://doi.org/10.4269/ajtmh.1995.52.536.

12. Diro E, Lynen L, Ritmeijer K, Boelaert M, Hailu A, van Griensven J. 2014. Visceral Leishmaniasis and HIV coinfection in East Africa. PLoS Negl Trop Dis 8:e2869. https://doi.org/10.1371/journal.pntd.0002869.

13. Mbongo N, Loiseau PM, Billion MA, Robert-Gero M. 1998. Mechanism of amphotericin B resistance in Leishmania donovani promastigotes. Antimicrob Agents Chemother 42:352–357. https://doi.org/10.1128/AAC.42.2.352.

14. Purkait B, Kumar A, Nandi N, Sardar AH, Das S, Kumar S, Pandey K, Ravidas V, Kumar M, De T, Singh D, Das P. 2012. Mechanism of amphotericin B resistance in clinical isolates of Leishmania donovani. Antimicrob Agents Chemother 56:1031–1041. https://doi.org/10.1128/AAC.00030-11.

15. Pountain AW, Weidt SK, Regnault C, Bates PA, Donachie AM, Dickens NJ, Barrett MP. 2019. Genomic instability at the locus of sterol C24-methyltransferase promotes amphotericin B resistance in Leishmania parasites. PLoS Negl Trop Dis 13:e0007052. https://doi.org/10.1371/journal.pntd.0007052.

16. Mwenechanya R, Kovářová J, Dickens NJ, Mudaliar M, Herzyk P, Vincent IM, Weidt SK, Burgess KE, Burchmore RJS, Pountain AW, Smith TK, Creek DJ, Kim D-H, Lepesheva GI, Barrett MP. 2017. Sterol 14alpha-demethylase mutation leads to amphotericin B resistance in Leishmania mexicana. PLoS Negl Trop Dis 11:e0005649. https://doi.org/10.1371/journal.pntd.0005649.

17. Cruz A, Beverley SM. 1990. Gene replacement in parasitic protozoa. Nature 348:171–173. https://doi.org/10.1038/348171a0.

18. Mukherjee S, Xu W, Hsu FF, Patel J, Huang J, Zhang K. 2019. Sterol methyltransferase is required for optimal mitochondrial function and virulence in Leishmania major. Mol Microbiol 111:65–81. https://doi.org/10.1111/mmi.14139.

19. Xu W, Hsu F-F, Baykal E, Huang J, Zhang K. 2014. Sterol biosynthesis is required for heat resistance but not extracellular survival in Leishmania. PLoS Pathog 10:e1004427. https://doi.org/10.1371/journal.ppat.1004427.

20. McConville MJ, Thomas-Oates JE, Ferguson MA, Homans SW. 1990. Structure of the lipophosphoglycan from Leishmania major. J Biol Chem 265:19611–19623.

21. Kelly SL, Lamb DC, Kelly DE, Manning NJ, Loeffler J, Hebart H, Schumacher U, Einsele H. 1997. Resistance to fluconazole and cross-resistance to amphotericin B in Candida albicans from AIDS patients caused by defective sterol delta5,6-desaturation. FEBS Lett 400:80–82. https://doi.org/10.1016/s0014-5793(96)01360-9.

22. Young LY, Hull CM, Heitman J. 2003. Disruption of ergosterol biosynthesis confers resistance to amphotericin B in Candida lusitaniae. Antimicrob Agents Chemother 47:2717–2724. https://doi.org/10.1128/aac.47.9.2717-2724.2003.

23. Arthington BA, Bennett LG, Skatrud PL, Guynn CJ, Barbuch RJ, Ulbright CE, Bard M. 1991. Cloning, disruption and sequence of the gene encoding yeast C-5 sterol desaturase. Gene 102:39–44. https://doi.org/10.1016/0378-1119(91)90535-j.

24. Matsushima M, Inazawa J, Takahashi E, Suzumori K, Nakamura Y. 1996. Molecular cloning and mapping of a human cDNA (SC5DL) encoding a protein homologous to fungal sterol-C5-desaturase. Cytogenet Cell Genet 74:252–254. https://doi.org/10.1159/000134427.

25. Brumfield KM, Moroney JV, Moore TS, Simms TA, Donze D. 2010. Functional characterization of the Chlamydomonas reinhardtii ERG3 ortholog, a gene involved in the biosynthesis of ergosterol. PLoS One 5:e8659. https://doi.org/10.1371/journal.pone.0008659.

26. Gachotte D, Husselstein T, Bard M, Lacroute F, Benveniste P. 1996. Isolation and characterization of an Arabidopsis thaliana cDNA encoding a delta 7-sterol-C-5-desaturase by functional complementation of a defective yeast mutant. Plant J 9:391–398. https://doi.org/10.1046/j.1365-313x.1996.09030391.x.

27. Osumi T, Nishino T, Katsuki H. 1979. Studies on the delta 5-desaturation in ergosterol biosynthesis in yeast. J Biochem 85:819–826.

28. Poklepovich TJ, Rinaldi MA, Tomazic ML, Favale NO, Turkewitz AP, Nudel CB, Nusblat AD. 2012. The cytochrome b5 dependent C-5(6) sterol desaturase DES5A from the endoplasmic reticulum of Tetrahymena thermophila complements ergosterol biosynthesis mutants in Saccharomyces cerevisiae. Steroids 77:1313–1320. https://doi.org/10.1016/j.steroids.2012.08.015.

29. Darnet S, Schaller H. 2019. Metabolism and biological activities of 4-methyl-sterols. Molecules 24:451. https://doi.org/10.3390/molecules24030451.

30. Waterman MR, Lepesheva GI. 2005. Sterol 14 alpha-demethylase, an abundant and essential mixed-function oxidase. Biochem Biophys Res Commun 338:418–422. https://doi.org/10.1016/j.bbrc.2005.08.118.

31. Smith SJ, Parks LW. 1993. The ERG3 gene in Saccharomyces cerevisiae is required for the utilization of respiratory substrates and in heme-deficient cells. Yeast 9:1177–1187. https://doi.org/10.1002/yea.320091104.

32. Kamthan A, Kamthan M, Datta A. 2017. Expression of C-5 sterol desaturase from an edible mushroom in fission yeast enhances its ethanol and thermotolerance. PLoS One 12:e0173381. https://doi.org/10.1371/journal.pone.0173381.

33. Alcazar-Fuoli L, Mellado E, Garcia-Effron G, Buitrago MJ, Lopez JF, Grimalt JO, Cuenca-Estrella JM, Rodriguez-Tudela JL. 2006. Aspergillus fumigatus C-5 sterol desaturases Erg3A and Erg3B: role in sterol biosynthesis and antifungal drug susceptibility. Antimicrob Agents Chemother 50:453–460. https://doi.org/10.1128/AAC.50.2.453-460.2006.

34. Sanglard D, Ischer F, Parkinson T, Falconer D, Bille J. 2003. Candida albicans mutations in the ergosterol biosynthetic pathway and resistance to several antifungal agents. Antimicrob Agents Chemother 47:2404–2412. https://doi.org/10.1128/aac.47.8.2404-2412.2003.

35. Bangs JD, Uyetake L, Brickman MJ, Balber AE, Boothroyd JC. 1993. Molecular cloning and cellular localization of a BiP homologue in Trypanosoma brucei. Divergent ER retention signals in a lower eukaryote. J Cell Sci 105:1101–1113.

36. Sacks DL, Perkins PV. 1984. Identification of an infective stage of Leishmania promastigotes. Science 223:1417–1419. https://doi.org/10.1126/science.6701528.

37. Sundar S, Chakravarty J. 2010. Liposomal amphotericin B and leishmaniasis: dose and response. J Glob Infect Dis 2:159–166. https://doi.org/10.4103/0974-777X.62886.

38. Podinovskaia M, Descoteaux A. 2015. Leishmania and the macrophage: a multifaceted interaction. Future Microbiol 10:111–129. https://doi.org/10.2217/fmb.14.103.

39. Moradin N, Descoteaux A. 2012. Leishmania promastigotes: building a safe niche within macrophages. Front Cell Infect Microbiol 2:121. https://doi.org/10.3389/fcimb.2012.00121.

40. Pal DS, Abbasi M, Mondal DK, Varghese BA, Paul R, Singh S, Datta R. 2017. Interplay between a cytosolic and a cell surface carbonic anhydrase in pH homeostasis and acid tolerance of Leishmania. J Cell Sci 130:754–766. https://doi.org/10.1242/jcs.199422.

41. Docampo R, de Souza W, Miranda K, Rohloff P, Moreno SN. 2005. Acidocalcisomes—conserved from bacteria to man. Nat Rev Microbiol 3:251–261. https://doi.org/10.1038/nrmicro1097.

42. Docampo R, Jimenez V, Lander N, Li ZH, Niyogi S. 2013. New insights into roles of acidocalcisomes and contractile vacuole complex in osmoregulation in protists. Int Rev Cell Mol Biol 305:69–113. https://doi.org/10.1016/B978-0-12-407695-2.00002-0.

43. Rodrigues CO, Scott DA, Docampo R. 1999. Presence of a vacuolar H+-pyrophosphatase in promastigotes of Leishmania donovani and its localization to a different compartment from the vacuolar H+-ATPase. Biochem J 340:759–766. https://doi.org/10.1042/0264-6021:3400759.

44. Lemercier G, Dutoya S, Luo S, Ruiz FA, Rodrigues CO, Baltz T, Docampo R, Bakalara N. 2002. A vacuolar-type H+-pyrophosphatase governs maintenance of functional acidocalcisomes and growth of the insect and mammalian forms of Trypanosoma brucei. J Biol Chem 277:37369–37376. https://doi.org/10.1074/jbc.M204744200.

45. Brown DA, London E. 1998. Structure and origin of ordered lipid domains in biological membranes. J Membr Biol 164:103–114. https://doi.org/10.1007/s002329900397.

46. Kelleher M, Bacic A, Handman E. 1992. Identification of a macrophage-binding determinant on lipophosphoglycan from Leishmania major promastigotes. Proc Natl Acad Sci U S A 89:6–10. https://doi.org/10.1073/pnas.89.1.6.

47. De Ibarra A, Howard J, Snary D. 1982. Monoclonal antibodies to Leishmania tropica major: specificities and antigen location. Parasitology 85:523–531. https://doi.org/10.1017/S0031182000056304.

48. Sacks DL. 1992. The structure and function of the surface lipophosphoglycan on different developmental stages of Leishmania promastigotes. Infect Agents Dis 1:200–206.

49. Dobson DE, Scholtes LD, Valdez KE, Sullivan DR, Mengeling BJ, Cilmi S, Turco SJ, Beverley SM. 2003. Functional identification of galactosyltransferases (SCGs) required for species-specific modifications of the lipophosphoglycan adhesin controlling Leishmania major-sand fly interactions. J Biol Chem 278:15523–15531. https://doi.org/10.1074/jbc.M301568200.

50. Dobson DE, Mengeling BJ, Cilmi S, Hickerson S, Turco SJ, Beverley SM.

2003. Identification of genes encoding arabinosyltransferases (SCA) mediating developmental modifications of lipophosphoglycan required for sand fly transmission of Leishmania major. J Biol Chem 278:28840–28848. https://doi.org/10.1074/jbc.M302728200.

51. Spath GF, Epstein L, Leader B, Singer SM, Avila HA, Turco SJ, Beverley SM. 2000. Lipophosphoglycan is a virulence factor distinct from related glycoconjugates in the protozoan parasite Leishmania major. Proc Natl Acad Sci U S A 97:9258–9263. https://doi.org/10.1073/pnas.160257897.

52. Spath GF, Lye LF, Segawa H, Sacks DL, Turco SJ, Beverley SM. 2003. Persistence without pathology in phosphoglycan-deficient Leishmania major. Science 301:1241–1243. https://doi.org/10.1126/science.1087499.

53. Tolson DL, Turco SJ, Beecroft RP, Pearson TW. 1989. The immunochemical structure and surface arrangement of Leishmania donovani lipophosphoglycan determined using monoclonal antibodies. Mol Biochem Parasitol 35:109–118. https://doi.org/10.1016/0166-6851(89)90113-8.

54. McConville MJ, Schnur LF, Jaffe C, Schneider P. 1995. Structure of Leishmania lipophosphoglycan: inter- and intra-specific polymorphism in Old World species. Biochem J 310:807–818. https://doi.org/10.1042/bj3100807.

55. Soares RP, Barron T, McCoy-Simandle K, Svobodova M, Warburg A, Turco SJ. 2004. Leishmania tropica: intraspecific polymorphisms in lipophosphoglycan correlate with transmission by different Phlebotomus species. Exp Parasitol 107:105–114. https://doi.org/10.1016/j.exppara.2004.05.001.

56. McConville MJ, Turco SJ, Ferguson MA, Sacks DL. 1992. Developmental modification of lipophosphoglycan during the differentiation of Leishmania major promastigotes to an infectious stage. EMBO J 11:3593–3600. https://doi.org/10.1002/j.1460-2075.1992.tb05443.x.

57. Turco SJ, Descoteaux A. 1992. The lipophosphoglycan of Leishmania parasites. Annu Rev Microbiol 46:65–94. https://doi.org/10.1146/annurev.mi.46.100192.000433.

58. McConville MJ, Homans SW, Thomas-Oates JE, Dell A, Bacic A. 1990. Structures of the glycoinositolphospholipids from Leishmania major. A family of novel galactofuranose-containing glycolipids. J Biol Chem 265:7385–7394.

59. Assis RR, Ibraim IC, Noronha FS, Turco SJ, Soares RP. 2012. Glycoinositolphospholipids from Leishmania braziliensis and L. infantum: modulation of innate immune system and variations in carbohydrate structure. PLoS Negl Trop Dis 6:e1543. https://doi.org/10.1371/journal.pntd.0001543.

60. Medina J, Rodrigues J, De Souza W, Atella G, Barrabin H. 2012. Tomatidine promotes the inhibition of 24-alkylated sterol biosynthesis and mitochondrial dysfunction in Leishmania amazonensis promastigotes. Parasitology 139:1253–1265. https://doi.org/10.1017/S0031182012000522.

61. Kessler RL, Soares MJ, Probst CM, Krieger MA. 2013. Trypanosoma cruzi response to sterol biosynthesis inhibitors: morphophysiological alterations leading to cell death. PLoS One 8:e55497. https://doi.org/10.1371/journal.pone.0055497.

62. Pérez-Moreno G, Sealey-Cardona M, Rodrigues-Poveda C, Gelb MH, Ruiz-Pérez LM, Castillo-Acosta V, Urbina JA, González-Pacanowska D. 2012. Endogenous sterol biosynthesis is important for mitochondrial function and cell morphology in procyclic forms of Trypanosoma brucei. Int J Parasitol 42:975–989. https://doi.org/10.1016/j.ijpara.2012.07.012.

63. Schmidt CL, Grey M, Schmidt M, Brendel M, Henriques JA. 1999. Allelism of Saccharomyces cerevisiae genes PSO6, involved in survival after 3-CPs+ UVA induced damage, and ERG3, encoding the enzyme sterol C-5 desaturase. Yeast 15:1503–1510. https://doi.org/10.1002/(SICI)1097-0061(199910)15:14<1503::AID-YEA481>3.0.CO;2-W.

64. Crowley LC, Christensen ME, Waterhouse NJ. 2016. Measuring mitochondrial transmembrane potential by TMRE staining. Cold Spring Harb Protoc 2016:pdb.prot087361. https://doi.org/10.1101/pdb.prot087361.

65. Cardenas D, Carter PM, Nation CS, Pizarro JC, Guidry J, Aiyar A, Kelly BL. 2015. LACK, a RACK1 ortholog, facilitates cytochrome c oxidase subunit expression to promote Leishmania major fitness. Mol Microbiol 96:95–109. https://doi.org/10.1111/mmi.12924.

66. Capul AA, Hickerson S, Barron T, Turco SJ, Beverley SM. 2007. Comparisons of mutants lacking the Golgi UDP-galactose or GDP-mannose transporters establish that phosphoglycans are important for promasti-

gote but not amastigote virulence in Leishmania major. Infect Immun 75:4629–4637. https://doi.org/10.1128/IAI.00735-07.

67. Forestier CL, Gao Q, Boons GJ. 2014. Leishmania lipophosphoglycan: how to establish structure-activity relationships for this highly complex and multifunctional glycoconjugate? Front Cell Infect Microbiol 4:193. https://doi.org/10.3389/fcimb.2014.00193.

68. Alvar J, Croft S, Olliaro P. 2006. Chemotherapy in the treatment and control of leishmaniasis. Adv Parasitol 61:223–274. https://doi.org/10.1016/S0065-308X(05)61006-8.

69. Lachaud L, Bourgeois N, Plourde M, Leprohon P, Bastien P, Ouellette M. 2009. Parasite susceptibility to amphotericin B in failures of treatment for visceral leishmaniasis in patients coinfected with HIV type 1 and Leishmania infantum. Clin Infect Dis 48:e16–e22. https://doi.org/10.1086/595710.

70. Durand R, Paul M, Pratlong F, Rivollet D, Dubreuil-Lemaire ML, Houin R, Astier A, Deniau M. 1998. Leishmania infantum: lack of parasite resistance to amphotericin B in a clinically resistant visceral leishmaniasis. Antimicrob Agents Chemother 42:2141–2143. https://doi.org/10.1128/AAC.42.8.2141.

71. McCall LI, El Aroussi A, Choi JY, Vieira DF, De Muylder G, Johnston JB, Chen S, Kellar D, Siqueira-Neto JL, Roush WR, Podust LM, McKerrow JH. 2015. Targeting ergosterol biosynthesis in Leishmania donovani: essentiality of sterol 14 alpha-demethylase. PLoS Negl Trop Dis 9:e0003588. https://doi.org/10.1371/journal.pntd.0003588.

72. Kapler GM, Coburn CM, Beverley SM. 1990. Stable transfection of the human parasite Leishmania major delineates a 30-kilobase region sufficient for extrachromosomal replication and expression. Mol Cell Biol 10:1084–1094. https://doi.org/10.1128/mcb.10.3.1084.

73. Spath GF, Beverley SM. 2001. A lipophosphoglycan-independent method for isolation of infective Leishmania metacyclic promastigotes by density gradient centrifugation. Exp Parasitol 99:97–103. https://doi.org/10.1006/expr.2001.4656.

74. Folch J, Lees M, Stanley GS. 1957. A simple method for the isolation and purification of total lipids from animal tissues. J Biol Chem 226:497–509.

75. Bolte S, Cordelieres FP. 2006. A guided tour into subcellular colocalization analysis in light microscopy. J Microsc 224:213–232. https://doi.org/10.1111/j.1365-2818.2006.01706.x.

76. Vieira L, Lavan A, Dagger F, Cabantchik ZI. 1994. The role of anions in pH regulation of Leishmania major promastigotes. J Biol Chem 269:16254–16259.

77. Pal DS, Mondal DK, Datta R. 2015. Identification of metal dithiocarbamates as a novel class of antileishmanial agents. Antimicrob Agents Chemother 59:2144–2152. https://doi.org/10.1128/AAC.05146-14.

78. Manzano JI, Carvalho L, Perez-Victoria JM, Castanys S, Gamarro F. 2011. Increased glycolytic ATP synthesis is associated with tafenoquine resistance in Leishmania major. Antimicrob Agents Chemother 55:1045–1052. https://doi.org/10.1128/AAC.01545-10.

79. Huang G, Moreno SNJ, Docampo R. 2020. Isolation and characterization of acidocalcisomes from trypanosomatids. Methods Mol Biol 2116:673–688. https://doi.org/10.1007/978-1-0716-0294-2_40.

80. Ruiz FA, Rodrigues CO, Docampo R. 2001. Rapid changes in polyphosphate content within acidocalcisomes in response to cell growth, differentiation, and environmental stress in Trypanosoma cruzi. J Biol Chem 276:26114–26121. https://doi.org/10.1074/jbc.M102402200.

81. Connell ND, Medina-Acosta E, McMaster WR, Bloom BR, Russell DG. 1993. Effective immunization against cutaneous leishmaniasis with recombinant bacille Calmette-Guerin expressing the Leishmania surface proteinase gp63. Proc Natl Acad Sci U S A 90:11473–11477. https://doi.org/10.1073/pnas.90.24.11473.

82. Paranaíba LF, de Assis RR, Nogueira PM, Torrecilhas AC, Campos JH, Silveira A. C d O, Martins-Filho OA, Pessoa NL, Campos MA, Parreiras PM, Melo MN, Gontijo N. d F, Soares RPP. 2015. Leishmania enriettii: biochemical characterisation of lipophosphoglycans (LPGs) and glycoinositolphospholipids (GIPLs) and infectivity to Cavia porcellus. Parasit Vectors 8:31. https://doi.org/10.1186/s13071-015-0633-8.

83. Titus RG, Marchand M, Boon T, Louis J. 1985. A limiting dilution assay for quantifying Leishmania major in tissues of infected mice. Parasite Immunol 7:545–555. https://doi.org/10.1111/j.1365-3024.1985.tb00098.x.